Antibody Mass Escalation Study in Patients with Castration-Resistant Prostate Cancer Using ^{111}In-J591: Lesion Detectability and Dosimetric Projections for ^{90}Y Radioimmunotherapy

Neeta Pandit-Taskar[1,2], Joseph A. O'Donoghue[3], Michael J. Morris[4,5], Eze A. Wills[2], Lawrence H. Schwartz[1], Mithat Gonen[6], Howard I. Scher[4,5], Steven M. Larson[1,2], and Chaitanya R. Divgi[1,2]

[1]Nuclear Medicine Service, Department of Radiology, Memorial Sloan-Kettering Cancer Center, New York, New York; [2]Department of Radiology, Weill Medical College of Cornell University, New York, New York; [3]Department of Medical Physics, Memorial Sloan-Kettering Cancer Center, New York, New York; [4]Genitourinary Oncology Service, Department of Medicine, Memorial Sloan-Kettering Cancer Center, New York, New York; [5]Department of Medicine, Weill Medical College of Cornell University, New York, New York; and [6]Department of Biostatistics, Memorial Sloan-Kettering Cancer Center, New York, New York

J591, a monoclonal antibody that targets the external domain of the prostate-specific membrane antigen, has potential as an agent for radioimmunotherapy. A pilot trial was performed in patients with prostate cancer using repetitive administrations of escalating masses of J591. An analysis was performed to assess lesion detectability by ^{111}In-J591 γ-camera imaging compared with standard imaging methods and the effect of increasing antibody mass on lesion detectability, biodistribution, and dosimetry. **Methods:** Fourteen patients with metastatic prostate cancer received escalating amounts (10, 25, 50, and 100 mg) of J591 in a series of administrations each separated by 3 wk. All antibody administrations included a fixed amount of the radiolabeled antibody ^{111}In-1,4,7,10-tetraazacyclododecane-*N,N′,N″,N‴*-tetraacetic acid-J591 (^{111}In-DOTA-J591) (2 mg of J591 labeled with 185 MBq [5 mCi] of ^{111}In via the chelating agent DOTA). Three whole-body γ-camera scans with at least 1 SPECT scan together with multiple whole-body counting-rate measurements and serum activity-concentration measurements were obtained in all patients. Images were analyzed for distribution and lesion targeting. Estimates of clearance rates and liver and lesion uptake were made for each treatment cycle. These estimates were used to generate dosimetric projections for radioimmunotherapy with ^{90}Y-labeled J591. **Results:** A total of 80 lesions in 14 patients were detected. Both skeletal and soft-tissue diseases were targeted by the antibody as seen on ^{111}In-J591 scans. The antibody localized to 93.7% of skeletal lesions detected by conventional imaging. Clearance of radioactivity from the whole body, serum, and liver was dependent on antibody mass. Normalized average values of the ratio of residence times between lesion and liver for 10, 25, 50, and 100 mg of antibody were 1.0, 1.9, 3.2, and 4.0. Dosimetric projections for radioimmunotherapy with ^{90}Y-labeled J591 suggested similar absorbed doses to lesions for treatment at the maximally tolerated activity (MTA), irrespective of antibody mass. However, absorbed doses to liver at the MTA would be antibody mass–dependent with estimates of 20, 10, 7, and 5 Gy for 10, 25, 50, and 100 mg of J591. **Conclusion:** The proportion of the amount of antibody increased in lesions and decreased in the liver with increasing mass of administered antibody up to a dose of 50 mg. Proportional hepatic uptake continued to decrease with increasing antibody mass up to 100 mg. The optimal antibody mass for radioimmunotherapy would therefore appear to be greater than or equal to 50 mg.

Key Words: J591 antibody; prostate cancer; radioimmunotherapy; dosimetry

J Nucl Med 2008; 49:1066–1074
DOI: 10.2967/jnumed.107.049502

Prostate-specific membrane antigen (PSMA) is a transmembrane glycoprotein found on prostate epithelial cells. Both benign and malignant prostatic compared with nonprostatic tissues show excess PSMA expression (*1*). PSMA expression appears to be greatest in primary prostate adenocarcinoma and nodal metastasis (*2,3*). The radiolabeled anti-PSMA antibody capromab pendetide (ProstaScint; Cytogen Corp.) has been approved by the Food and Drug Administration for evaluation of metastatic prostate cancer by scintigraphic imaging. Capromab pendetide antibody targets an internal domain of PSMA and has been used in management of prostate cancer to detect metastatic disease and recurrence (*4,5*). J591 (Millennium Pharmaceuticals), a monoclonal IgG1 antibody that targets the external domain of PSMA (*6,7*), was derived from the original murine J591 by replacement of the B- and T-cell epitopes (*8*). J591 exhibits immune effector function, mainly by inducing antibody-dependent cellular cytotoxicity (*7*). The antibody can be conjugated to a variety of

Received Dec. 1, 2007; revision accepted Mar. 18, 2008.
For correspondence or reprints contact: Neeta Pandit-Taskar, Nuclear Medicine Service, Department of Radiology, Memorial Sloan-Kettering Cancer Center, 1275 York Ave., Box 77, New York, NY 10021.
E-mail: pandit-n@mskcc.org

radiometals using the chelating agent 1,4,7,10-tetraazacyclododecane-*N,N′,N″,N‴*-tetraacetic acid (DOTA) (*7,9*).

Pilot studies to evaluate safety and biodistribution in patients with prostate cancer and solid tumors with extensive neovasculature showed J591 was safe to administer, localized to bone and soft-tissue metastatic sites, and exhibited dose-dependent hepatic uptake (*10–14*).

In a phase I study evaluating ^{111}In-J591 in patients with prostate cancer, dose-dependent clearance for administered masses lower than 50 mg was seen; however, clearance rates did not differ after repeated administrations over a 4-wk period (*15*).

The feasibility of radioimmunotherapy using J591 has been explored. A phase I, dose-escalation radioimmunotherapy study using ^{177}Lu-J591 (370–2,590 MBq/m^2 or 10–70 mCi/m^2; 10 mg/m^2 antibody) showed biodistribution and clearance kinetics similar to those of ^{111}In-labeled J591 antibody (*13*). Bone marrow was the dose-limiting organ, with liver as the probable second critical organ for toxicity (*13,14*). The radiation dose to bone marrow was estimated as 0.32 ± 0.1 mGy/MBq whereas that to liver was estimated as 2.1 ± 0.6 mGy/MBq (*14*).

We have previously reported decreasing liver uptake with increasing antibody mass (*15,16*). In the current study, we present an analysis of lesion detection and targeting of ^{111}In-J591 to hormone-refractory prostate cancer, with particular emphasis on the effect of escalating antibody mass on lesion detection, biodistribution, and pharmacokinetics. Unique features of this analysis include the comparative lesion and normal tissue pharmacokinetics and dosimetry and the impact of increasing antibody mass on lesion detection with ^{111}In-J591. We also evaluated the feasibility of using this antibody for targeted radionuclide therapy by making dosimetric projections for ^{90}Y-J591 on the basis of the data measured for ^{111}In-J591.

MATERIALS AND METHODS

Patients

A total of 14 patients with metastatic biopsy-proven prostate cancer were studied. All patients had progression of disease as determined by an increase in prostate-specific antigen (PSA) and in lesions on bone scans or either an increase in the number of lesions or more than a 25% increase in bidimensional lesion measurement on CT scans. A minimum PSA of 4 ng/dL was required, and a 25% rise in PSA over 2 measurements obtained 4 wk apart or 3 measurements performed 1 wk apart was considered significant for progression. All patients had received previous therapy with hormones. All patients provided written informed consent, and the protocol was approved by the Institutional Review Board of Memorial Sloan-Kettering Cancer Center, the sole study site.

Study Design

This study featured a novel design of intrapatient mass escalation of administered antibody as described previously (*15*). A total of 14 patients were entered into the study, with each patient receiving cycles of J591 with progressively increasing antibody mass: 12 patients received all 4 antibody infusions, 1 patient received 3 antibody infusions (10, 50, and 100 mg), and 1 patient received 2 antibody infusions (10 and 25 mg). Starting at 10 mg, the mass of administered antibody was increased at 3-wk intervals to 25 mg on day 22, 50 mg on day 43, and 100 mg on day 64. All administrations, irrespective of the total antibody mass, included a fixed amount of radiolabeled antibody ^{111}In-DOTA-J591 (2 mg of J591 labeled with 185 MBq [5 mCi] of ^{111}In via the chelating agent DOTA) (*15*). All infusions were administered at a rate of at least 5 mg of antibody/min (*15*).

Antibody Radiolabeling

J591 antibody was conjugated with DOTA by direct coupling of 1 of the 4 carboxylic acid groups of DOTA to the primary amines present in the protein structure and subsequently labeled with ^{111}In as described previously (*9*). The specific activity of ^{111}In-DOTA-J591 was approximately 220 MBq/mg (7.6 mCi/mg). All radiolabeled material was checked for radiochemical purity using instant thin-layer chromotography and immunoreactivity using previously described methods (*15*). The radiolabeling yield was more than 85%, radiochemical purity was 99%, and immunoreactivity was 72% or higher for all administered doses.

γ-Camera Imaging

Anterior and posterior whole-body planar scans were acquired on a dual-head γ-camera (Philips Inc.) using dual-energy acquisition centered at 171 and 245 keV with 20% windows. Each patient underwent at least 3 whole-body scans performed on the day of infusion, between days 2 and 4, and between days 5 and 7, with separate scans of an ^{111}In standard of known activity and background acquired contemporaneously. All patients also underwent SPECT scans (64 steps, 40 s each) of the chest, abdomen, or pelvis to further evaluate sites of uptake from planar imaging or known areas of disease from conventional imaging. SPECT images were constructed using iterative reconstruction and attenuation correction.

Image Interpretation and Lesion Detection

All images were reviewed by nuclear medicine physicians unaware of the other conventional imaging results for tumor targeting. For each patient, anterior and posterior whole-body images obtained after each antibody infusion at 3 time points and SPECT images were visually analyzed. All visualized areas of uptake were graded on a scale of 1–5 (1, negative; 2, probably negative; 3, equivocal; 4, probably positive; 5, definitely positive). All such areas of uptake were recorded. Baseline CT scans and ^{99m}Tc-methylene diphosphonate bone scans were reviewed for lesions by separate radiologists who were unaware of the results of the antibody scans. All lesions detected by antibody scans and CT or bone scanning were recorded separately and then compared.

Whole-Body Clearance Measurements

Anterior and posterior whole-body counting rates were measured by a 12.7-cm (5-in)-thick sodium iodide scintillation detector probe at a fixed geometry (3 m from probe to patient). A total of 5–7 measurements were made on each patient from the day of infusion for up to 7 d after antibody administration. The net counting rates at later times were normalized to the rates immediately after administration (taken as the 100% value) to yield percentage retained activities. These data were used to generate clearance curves and calculate kinetic parameters.

Serum Clearance Measurements

Typically 5 serum samples were obtained: a sample on the day of antibody administration at 5, 15, 30, 60, and 120 min after antibody infusion and a sample on at least 3 occasions for up to 7 d after administration. Aliquots of serum were measured in duplicate using a γ-well counter (LKB Wallac, Inc.) together with appropriate ^{111}In standards. Measured activity concentrations were converted to percentage injected dose per liter and used to generate clearance curves and calculate pharmacokinetic parameters.

Derivation of Whole-Body and Serum Kinetic Parameters

Biologic and effective clearance rates and corresponding half-times were estimated for each treatment cycle using a software application (SAMM II; SAAM Institute Inc.) (*17*). A monoexponential function was fitted to the whole-body data, whereas both mono- and biexponential functions were fitted to the serum data. Subsequently, whole-body and serum residence times, τ, were calculated according to the formula $\tau = \tilde{A}/A_0$, where $\tilde{A}$ is the cumulated activity (estimated by integration of the time–activity curve) and A_0 is the administered activity.

Determination of Uptake in Lesions and Liver

Regions of interest (ROIs) were drawn on anterior and posterior γ-camera images to encompass the whole body, on selected lesions that were clearly seen on both anterior and posterior images and were away from the site of the blood pool, on the whole liver, and on normal-tissue background. Typically ROIs were initially drawn on the latest images acquired after 50- or 100-mg antibody infusions (where lesions were generally most clearly seen) and then copied and pasted to all other image sets. In all, a total of 24 lesions in 14 patients were examined. Background-corrected geometric mean counts in lesion and liver ROIs were computed and expressed as proportions of the geometric mean whole-body count. These were converted to proportions of administered activity using the effective whole-body clearance curve derived from probe measurement. Residence times in lesions and liver were then estimated by trapezoidal integration. Areas under the terminal portions of the time–activity curves were calculated by extrapolation from the last measured estimate using the apparent terminal clearance rate or physical decay, whichever rate was the shorter.

To assess antibody mass–dependent variations in lesion or liver uptake, a relative uptake parameter was used. Relative uptake was defined as the ratio of residence time in lesions or liver for a particular antibody mass to residence time for an antibody mass of 10 mg. The use of relative uptakes calculated for individual patients minimizes the influence of interpatient differences and enables more optimal paired statistical comparisons between different antibody masses.

Normal-Tissue Dosimetry

Absorbed radiation doses to liver, red marrow, and whole body for ^{111}In-DOTA-J591 were estimated using the OLINDA/EXM software application (*18*). The input data were residence times for liver, red marrow, and remainder of body. Residence times for red marrow were derived from serum residence times using standard assumptions (*19*), namely a proportion of 0.19 of red marrow with a total mass of 1.12 kg composed of extracellular fluid in equilibrium with serum. On this basis, $\tau_{RM} = 0.21\tau_{serum}$, where τ_{serum} is the per-liter value. The residence time for the remainder of the body was derived by subtracting liver and red marrow residence times from the whole-body residence time. Normal-tissue doses were calculated for each patient on a per-cycle basis using individualized kinetics. No adjustments to standard adult male phantom organ masses were made.

To assess the potential utility of radioimmunotherapy using ^{90}Y-J591, the projected absorbed doses to normal tissues were estimated, assuming identical biodistribution between ^{111}In- and ^{90}Y-labeled antibodies. Residence times for ^{90}Y-J591 were derived in a similar manner to the procedure used for ^{111}In-labeled J591, adjusted for the difference in physical half-lives.

Assessment of Targeting Specificity

For each treatment cycle, the ratios of residence time in lesion to those in liver and the whole body were calculated. The lesion-to-liver ratio represents targeting specificity to the main antibody sink, whereas the lesion–to–whole-body ratio represents a more generalized assessment of targeting specificity. These ratios were subsequently normalized for each lesion to the value for a 10-mg antibody dose. Variations in these ratios with antibody mass may be due to changes in uptake or retention in lesions, liver, and whole body, either individually or together.

Projected Absorbed Doses to Lesions for ^{90}Y Radioimmunotherapy

Lesion dimensions were estimated from CT scans for 18 lesions in 12 patients. Lesion volumes were calculated assuming ellipsoidal geometry, and lesion mass was derived assuming unit density. Subsequently, lesion residence times, corrected for the difference in half-life between ^{90}Y and ^{111}In, were assigned to the CT-derived lesion masses.

Absorbed doses to lesions per unit of administered activity (D_l) for ^{90}Y, due only to self-irradiation, were calculated according to the formula $D_l = \Delta\tau_l\varphi_l/m_l$, where Δ (0.54 g Gy/MBq/h) is the absorbed dose per unit of cumulated activity concentration for ^{90}Y, τ_l is the ^{90}Y-equivalent lesion residence time, φ_l is the lesion size–dependent absorbed fraction for ^{90}Y, and m_l is the estimated lesion mass. To estimate absorbed fractions, the equivalent lesion spheric radius (for spheres of equal volume to ellipsoids, with axes given by the CT lesion measurements) was used to look up φ for ^{90}Y from the values tabulated by Bardiès and Chatal (*20*).

Statistics

Parameter estimates were quoted in terms of mean values and associated SEs. The statistical significance of differences between groups was assessed using paired *t* tests. For lesion detection, detection rates of the 3 modalities under investigation were compared using McNemar test. The proportion true-positive for each test was evaluated using clinical and radiographic follow-up as the gold standard. Binomial confidence intervals were computed using the Clopper-Pearson method. Some patients contributed more than 1 observation, and the resulting clustered data were analyzed using methods described by Gonen et al. (*21*).

RESULTS

Fourteen patients with known castration-resistant prostate cancer were treated with ^{111}In-J591 (Table 1). ^{111}In-J591 antibody scans were positive in all patients for either bone or soft-tissue lesions (Fig. 1). A total of 90 lesions including 80 bone lesions and 10 soft-tissue lesions were detected by either conventional imaging (CT or bone scanning) or antibody imaging. Soft-tissue lesions involved

TABLE 1
Lesion Distribution and Detection in Patients

Data	*n*
Patients	
Total	14
Bone metastasis	14
Nodal metastasis	3
Other organ metastasis	2
Scan positive	14
CT scan positive	14
Lesions	
Total lesions	90
Bone	80
Lymph nodes and organs (soft tissue)	10
Concordance: bone lesions	
CT or bone scan positive, Ab scan positive	54
CT or bone scan positive, Ab scan negative	8
CT and bone scan negative, Ab scan positive	18
Concordance: soft-tissue lesions	
CT scan positive, Ab scan positive	5
CT scan positive, Ab scan negative	3
CT scan negative, Ab scan positive	2

Ab = antibody.

lymph nodes ($n = 7$) and lung, prostate, and seminal vesicle ($n = 1$ each). A total of 56 bone lesions were detected by CT or bone scanning, and 8 soft-tissue lesions were seen by CT scanning.

Fifty-four (67.5%) osseous lesions were seen on bone scans and 72 (91.25%) on antibody scans (Table 2). A total of 32 skeletal lesions were detected on CT scans, 6 (7.5%) bony lesions seen on bone scans were not seen on antibody imaging, and 18 (22.5%) lesions seen on antibody scans were not detected on bone or CT scans. There was a statistically significant difference for detection of lesions between the imaging modalities (adjusted McNemar χ^2, $P = 0.01$). Of the 18 bony lesions identified on antibody scans alone, 13 (16.25%) were confirmed as true lesions on follow-up bone or CT scans, performed within 4 mo after the antibody scan. Eight bony lesions were not seen on antibody scans but were seen on either bone or CT scans.

A total of 10 soft-tissue lesions were seen on CT scans or antibody scans, 8 soft-tissue lesions were detected on CT scans, and 7 lesions were detected on antibody scans alone (Table 2). Five lesions were seen on both CT and antibody imaging; CT detected 3 lesions not seen on antibody imaging, and antibody imaging alone detected 2 lesions.

Lesions were more evident on antibody scans obtained at later time points after each infusion (Fig. 1). Lesions were more detectable on scans obtained with later infusions with higher (50–100 mg) antibody masses (Fig. 2).

Uptake and Clearance from Whole Body, Serum, Liver, and Lesions

The clearance of activity from both whole body and serum conformed to monoexponential kinetics with no apparent separate fast and slow clearance phases. Summary statistics are provided in Table 3. For both whole body and serum, biologic half-times increased with increasing antibody mass. All intergroup differences with one exception were statistically significant ($P < 0.05$) by paired t test. The sole exception was the difference between whole-body biologic half-times for antibody masses of 50 and 100 mg, which fell just outside the significance threshold ($P \sim 0.08$).

Residence times for whole body, serum, liver, and lesions are also provided in Table 3. For whole body, serum, and lesions, residence times increased with increasing antibody mass, whereas for liver they decreased.

As described in "Methods and Materials," relative uptake parameters (the ratio of residence times normalized to the 10-mg level) were used to assess antibody mass–dependent variations in liver and lesion uptake. These are shown in Table 3. All intergroup differences for lesions, except those between antibody masses of 50 and 100 mg, and all intergroup differences for liver, except those between antibody masses of 25 and 50 mg, were statistically significant.

Normal-Tissue Dosimetry

Estimates of absorbed doses (in mGy/MBq) for whole body, red marrow, and liver are provided in Table 4. As described in "Materials and Methods," the values for ^{90}Y are projections based on the assumption of identical biologic behavior between ^{111}In- and ^{90}Y-labeled J591. All intergroup differences were statistically significant ($P < 0.05$) by paired t test with the following exceptions: for whole body and red marrow, 25 versus 100 mg and 50 versus 100 mg, respectively, and for liver, 25 versus 50 mg.

Targeting Specificity

Targeting specificity was assessed using the relative lesion-to-liver and lesion–to–whole-body residence time ratios. These are shown in Figure 3. The lesion–to–whole-body ratio reached a maximum for an antibody mass of 50 mg. In contrast, the lesion-to-liver ratio continued to increase up to the maximum antibody mass administered (100 mg). This latter finding was because of the continual decease in liver residence time rather than an increase in lesion residence time (Table 3).

Dosimetric Projections for ^{90}Y-Labeled J591

Projected absorbed doses (mGy/MBq) to lesions for ^{90}Y-J591 are included in Table 4. The values are for a subset of 15 lesions in 10 patients who received all 4 administration cycles. The trend here was similar to that observed for lesion residence time and relative uptake, with a general increase in lesion-absorbed dose from 10 to 50 mg but no further increase from 50 to 100 mg.

We have previously estimated that an absorbed dose to the red marrow of 1.85 Gy is close to clinical tolerance for a single administration of ^{131}I-labeled antibody (*22*). The average administered activities of ^{90}Y-J591 that would result in a red marrow–absorbed dose of 1.85 Gy were

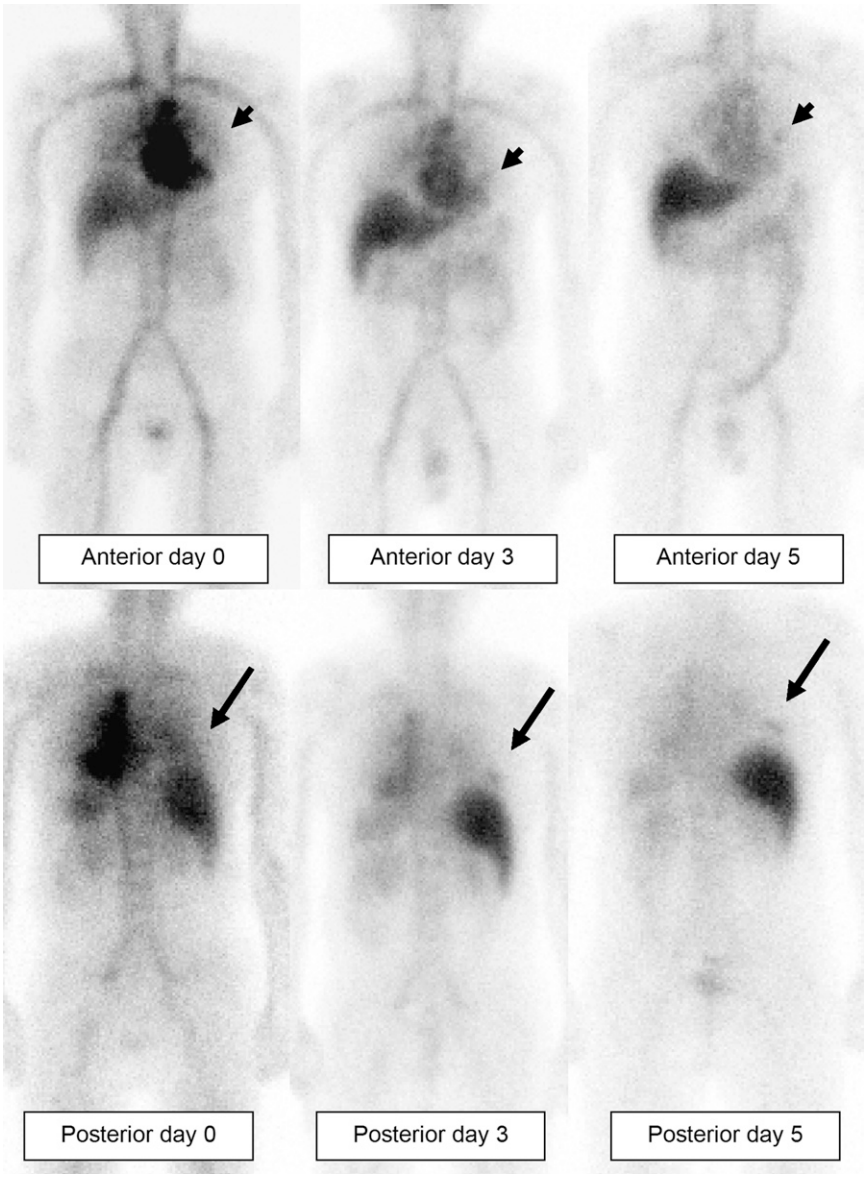

FIGURE 1. Patient with metastatic hormone-refractory prostate cancer, infused with ^{111}In-J591. Anterior and posterior whole-body images were acquired on day of infusion (day 0) and at 72 (day 3) and 120 h (day 5) after injection. Uptake of tracer is seen in left rib lesion anteriorly (arrowhead) and right rib lesion posteriorly (arrow). Both these lesions were not seen at all on day 0, faintly visualized on day 3, and clearly visualized on day 5.

calculated as a function of antibody mass. These activities, together with the corresponding average absorbed doses to liver and lesions, are shown in Table 5. Major differences are apparent between absorbed doses to liver for different values of antibody mass, with higher doses corresponding to lower antibody masses. In contrast, absorbed doses to lesions appear similar irrespective of antibody mass, because the dependencies between antibody mass and red marrow– and lesion-absorbed doses were similar. The lesion-absorbed dose estimates are very high (Table 5), most likely a consequence of the relatively small lesion mass estimates to which the γ-camera–derived residence times were assigned.

DISCUSSION

7E11, a murine antibody that targets the internal domain of PSMA, is widely used to visualize prostate cancer. This antibody (ProstaScint; Cytogen Corp.) is an imaging agent approved by the FDA for the detection of occult metastases from prostate cancer. However, it is unlikely that 7E11 is taken up by active viable disease, because of its binding to the internal domain of PSMA. J591 antibody preferentially binds to the external domain of PSMA and is thus more likely to detect viable prostate tissue.

This report represents an extension and refinement of the initial analysis (*15*), which reported on toxicity, antibody-dependent cellular cytotoxicity induction, and clinical antitumor effects in this patient group and provided a preliminary assessment of pharmacokinetics. One of the findings reported previously was that there was no difference in clearance characteristics between mixtures of radiolabeled and cold huJ591 antibody when administered either sequentially or concurrently (*15*). Thus, in the current report no distinction is made between patients on this basis, and

TABLE 2
Lesion Detection by Modality

Total skeletal lesions (all imaging)	No. skeletal lesions on bone scan only	No. skeletal lesions on bone or CT scan	No. of skeletal lesions on antibody scan only	Total soft-tissue lesions on CT/antibody scan	No. of soft-tissue lesions on CT scan only	No. of soft-tissue lesions on antibody scan only
7	1	3	7	3	2	3
6	3	3	6	0	0	0
8	5	6	6	0	0	0
8	7	7	7	0	0	0
1	1	1	1	0	0	0
6	3	3	6	0	0	0
3	3	3	2	0	0	0
9	8	9	8	0	0	0
5	3	5	4	0	0	0
7	5	5	7	0	0	0
1	0	1	0	4	4	2
4	2	2	3	3	2	2
6	6	6	6	0	0	0
9	7	7	9	0	0	0
80	54	61	72	10	8	7

the sole independent variable of interest is the mass of administered antibody. The previous study also reported that liver saturation was essentially complete for an antibody mass of 25 mg, on the basis of the lack of statistical significance between terminal values of the fraction of whole-body counts in the liver for antibody masses greater than or equal to 25 mg. The findings in the current study are more comprehensive and are based on analysis of full areas under the curve. As a proportion of the amount of antibody administered, hepatic uptake continues to decrease up to the highest mass administered (i.e., 100 mg).

We have quantitatively evaluated the uptake of ^{111}In-J591 in normal tissues and lesions and its dependency on the mass of antibody administered. Various parameters were examined including residence times, relative residence times, lesion-to-nonlesion residence time ratios, and absorbed dose. Irrespective of the parameters used, the findings were consistent and may be summarized as follows: increasing the mass of antibody administered results in an increased proportion of antibody retained in the circulation, in lesions, and in the whole body in general and a reduced proportion retained in the liver.

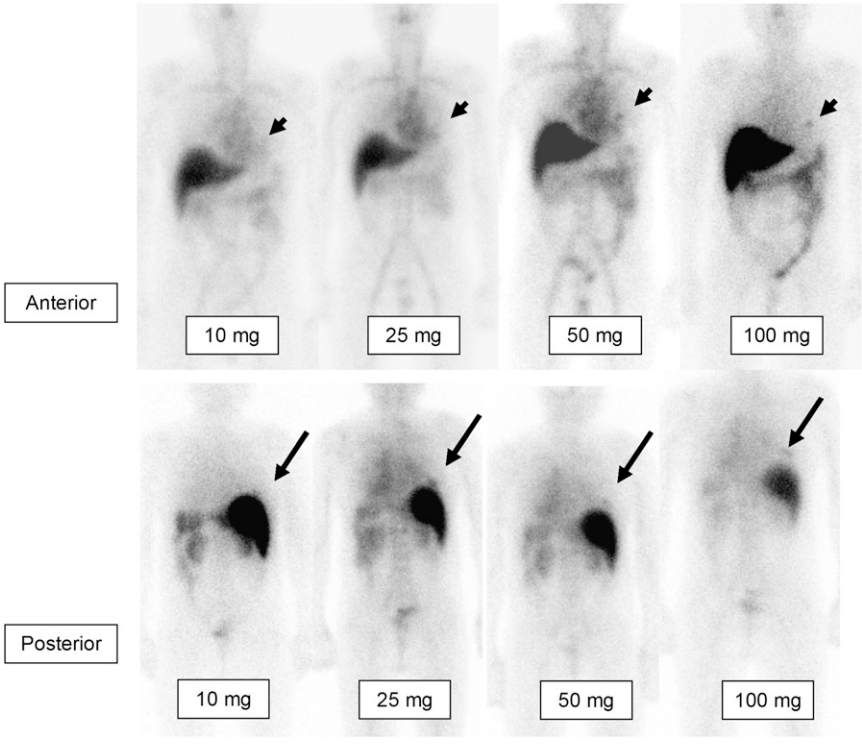

FIGURE 2. Patient with metastatic hormone-refractory prostate cancer. Anterior and posterior whole-body images were acquired on day of infusion (day 0) and at 72 (day 3) and 120 h (day 5) after injection for each of 10, 25, 50, and 100 mg of administered antibody. Tracer uptake is seen in left rib lesion anteriorly (arrowhead) and right rib lesion posteriorly (arrow). Both these lesions appear to be more clearly seen in scans with higher antibody infusions (50 and 100 mg) than with lower antibody mass infusions (10 and 25 mg).

TABLE 3
Summary of Kinetic and Uptake Data for Patients

Data	Administered antibody mass			
	10 mg	25 mg	50 mg	100 mg
Whole-body $T_{1/2\ biol}$ (d)*	8.5 (±0.8)	12.8 (±1.5)	17.7 (±2.2)	23.1 (±3.7)
Serum $T_{1/2\ biol}$ (d)†	0.96 (±0.07)	1.94 (±0.15)	2.78 (±0.22)	3.49 (±0.28)
Whole-body residence time (h)	71 (±2)	77 (±2)	82 (±2)	84 (±2)
Serum residence time (h)	24 (±1)	39 (±2)	47 (±2)	53 (±2)
Liver residence time (h)	21 (±1)	15 (±1)	13 (±2)	10 (±1)
Lesion residence time (h)	0.29 (±0.05)	0.38 (±0.07)	0.43 (±0.06)	0.45 (±0.08)
Relative liver uptake‡	1.0	0.70 (±0.03)	0.65 (±0.11)	0.48 (±0.07)
Relative lesion uptake§	1.0	1.32 (±0.04)	1.80 (±0.14)	1.67 (±0.13)

*All intergroup differences significant ($P < 0.05$) except 50 mg vs. 100 mg.
†All intergroup differences significant ($P < 0.05$).
‡All intergroup differences significant ($P < 0.05$) except 25 mg vs. 50 mg.
§All intergroup differences significant ($P < 0.05$) except 50 mg vs. 100 mg.
$T_{1/2\ biol}$ = biologic half-time.
Values are mean parameter estimates for each administered mass of huJ591. Quoted uncertainties are SEMs. Statistical significance of differences between groups assessed by paired *t* test.

These results are consistent with the hypothesis that the liver acts as a saturable sink for circulating antibody. Low amounts of antibody are rapidly removed from the circulation, leading to relatively low lesion uptake. As the amount of circulating antibody increases, the liver gradually saturates, a higher proportion remains in the circulation, and the relative lesion uptake increases.

For lesion detection, targeting is seen at all dose levels for lesions in both soft tissue and bone. However, in accordance with the quantitative uptake findings, increased detection of lesions with an increased mass amount of infused antibody was seen. Visually, more lesions were detected in delayed scans than on earlier scans (Fig.1). For any patient, lesions were better detected in the later infusions with a higher antibody mass (i.e., the third [50 mg] and fourth [100 mg] infusions) than in the earlier infusions (Fig. 2). The higher–antibody mass scans showed an increased number of lesions.

Antibody scans showed good targeting to skeletal disease. As compared with combined CT and bone scans for skeletal lesions, antibody scans detected an additional 13.7% lesions. Compared with bone scans alone, the results matched in 63% of lesions, whereas in 37% of lesions the results were discordant ($P = 0.01$). Compared with CT scans alone, antibody scans detected significantly more lesions ($P = 0.01$). There was 45% agreement between antibody and CT scan findings, whereas findings in 37% of lesions were discordant, with more lesions detected on antibody imaging.

Thirteen lesions seen only on antibody scans were confirmed as metastasis on follow-up conventional imaging. Eight lesions seen on bone or CT scans were not seen on antibody scans. Three of these lesions were in pelvic bones overlying sites of blood-pool activity in iliac or femoral vessel regions. Four lesions not seen on antibody imaging represented stable disease as assessed by follow-up

TABLE 4
Summary of Absorbed Dose Estimates (mGy/MBq) to Whole Body, Red Marrow, and Liver for ^{111}In-huJ591 and ^{90}Y-huJ591

Site	Isotope	Administered antibody mass			
		10 mg	25 mg	50 mg	100 mg
Whole body*	^{111}In	0.111 (±0.003)	0.119 (±0.003)	0.125 (±0.002)	0.123 (±0.006)
	^{90}Y	0.50 (±0.01)	0.55 (±0.01)	0.58 (±0.01)	0.57 (±0.03)
Red marrow*	^{111}In	0.111 (±0.004)	0.132 (±0.005)	0.146 (±0.004)	0.147 (±0.008)
	^{90}Y	0.55 (±0.03)	0.73 (±0.04)	0.86 (±0.04)	0.90 (±0.06)
Liver†	†^{111}In	0.75 (±0.03)	0.56 (±0.03)	0.48 (±0.04)	0.37 (±0.04)
	†^{90}Y	5.7 (±0.3)	4.1 (±0.3)	3.4 (±0.4)	2.5 (±0.3)
Lesion	^{90}Y	58 (±32)	78 (±45)	97 (±53)	95 (±53)

*All intergroup differences were statistically significant ($P < 0.05$) by paired *t* test except for 25 vs. 100 mg and 50 vs. 100 mg.
†All intergroup differences were statistically significant ($P < 0.05$) by paired *t* test except for 25 vs. 50 mg. Values quoted are mean (± SEM).

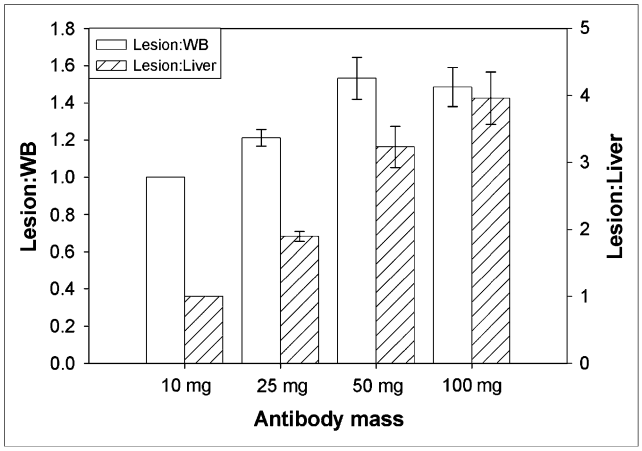

FIGURE 3. Relative residence time ratios between lesions and whole body or liver for different administered masses of J591. Error bars are SEM. All intergroup differences are statistically significant ($P < 0.05$) by paired *t* test except for lesion to whole body for 50 vs. 100 mg.

scans. Skeletal lesions missed on antibody scans were either small (<1.5 cm) or in areas with a high blood-pool background such as the mediastinum or pelvis. Overall, all 3 modalities differed significantly in detection rates.

The detection rate for soft tissue was low, likely related to small lesion size and location. None of 3 sites suspected for nodal disease on antibody scans were found to be true lesions on follow-up at 6 mo. These were located in the neck, pelvis, and inguinal regions and were likely related to prominent vascular activity. Among parenchymal lesions, antibody scans were able to detect only 1 lesion located in the peripheral lung. Detection of lung lesions near the cardiac blood pool would generally be limited. Other lesions not detected by antibody imaging were small (<10 mm) and in the prostate and seminal vesicles.

The potential of J591 as a molecular vector for radioimmunotherapy was assessed by examining the projected absorbed radiation doses for ^{90}Y-labeled antibody on the basis of the quantitative uptake parameters found for ^{111}In-labeled antibody. For a single therapeutic administration, the maximally tolerated activity (MTA) of ^{90}Y-J591 was defined by hematologic toxicity and would thus be expected to be determined by the absorbed dose to red marrow. On the basis of our analysis, it was expected that the MTA of ^{90}Y-J591 would be dependent on the mass of antibody administered. The differences in MTA for different antibody masses may be significant. For example, we estimated the MTA to be around 3,300 MBq (~90 mCi) for 10 mg of antibody, falling to around 2,000 MBq (~55 mCi) for 100 mg. Irrespective of the mass of antibody administered, treatment at the MTA would be expected to produce broadly similar absorbed doses to lesions. However, there would be major differences in absorbed dose to liver, ranging from about 20 Gy for 10 mg of antibody to about 5 Gy for 100 mg of antibody. The possibility of high doses to liver is important if multiple therapeutic administrations of radiolabeled antibody are contemplated. The hemopoietic system has a significant capacity for regeneration such that similar treatments could be repeated if sufficient time is provided between treatments to allow for recovery. In clinical radiobiologic terms, the liver is an example of a "late-responding" normal tissue characterized by long-term "memory" of latent radiation injury and a protracted time course for the expression of radiation damage. However, the liver may also experience significant sparing even for very high average radiation doses, if the dose distribution is spatially nonuniform. The use of ^{90}Y with its relatively long-range β-particle emissions would minimize the nonuniformity associated with the dose distribution.

A case could be made for defining the optimal mass of antibody to be 100 mg, as treatment at the MTA is predicted to result in the lowest absorbed dose to liver while delivering absorbed doses to lesions similar to lower antibody masses. However, it cannot be stated definitively if repetitive treatments at the 100-mg level would maintain a high lesion-targeting capability. In the current study, it was found that 100 mg of antibody provided high lesion uptake after successive administrations of 10, 25, and 50 mg. Thus, lesion targeting was maintained for a cumulative antibody mass of 185 mg (corresponding to an average of approximately 50 mg per administration).

Our data suggest that the optimal mass of J591 antibody for radioimmunotherapy over repeated cycles of treatment is at least 50 mg and may be as high as 100 mg.

TABLE 5
Administered Activities of ^{90}Y-J591 and Corresponding Estimates of Average Absorbed Doses

Parameter	Administered antibody mass			
	10 mg	25 mg	50 mg	100 mg
Activity of ^{90}Y for red marrow–absorbed dose of 1.85 Gy (MBq)	3,340	2,520	2,140	2,060
Projected absorbed dose to liver (Gy)	19.9	10.3	7.2	5.1
Projected absorbed dose to lesions (Gy)	193	195	208	196

CONCLUSION

J591 antibody targets both bone and soft-tissue lesions. The lesions are best targeted with higher mass amounts of antibody, most likely because of the saturation of liver uptake. Similarly, projected data for ^{90}Y-J591 treatment of metastatic lesions in prostate cancer patients suggest that higher antibody masses of at least 50 mg would be optimal for radioimmunotherapy.

ACKNOWLEDGMENTS

We thank Dr. Ronald Finn for providing radiolabeled antibody ^{111}In-J591. This study was funded in part by the

Prostate Cancer Foundation, the Sacerdote Fund, NCI grant CA10254, and the PepsiCo Foundation for Prostate Cancer.

REFERENCES

1. Murphy GP, Elgamal AA, Su SL, Bostwick DG, Holmes EH. Current evaluation of the tissue localization and diagnostic utility of prostate specific membrane antigen. *Cancer.* 1998;83:2259–2269.
2. Sweat SD, Pacelli A, Murphy GP, Bostwick DG. Prostate-specific membrane antigen expression is greatest in prostate adenocarcinoma and lymph node metastases. *Urology.* 1998;52:637–640.
3. Silver DA, Pellicer I, Fair WR, Heston WD, Cordon-Cardo C. Prostate-specific membrane antigen expression in normal and malignant human tissues. *Clin Cancer Res.* 1997;3:81–85.
4. Rosenthal SA, Haseman MK, Polascik TJ. Utility of capromab pendetide (ProstaScint) imaging in the management of prostate cancer. *Tech Urol.* 2001;7:27–37.
5. Petronis JD, Regan F, Lin K. Indium-111 capromab pendetide (ProstaScint) imaging to detect recurrent and metastatic prostate cancer. *Clin Nucl Med.* 1998;23:672–677.
6. Smith-Jones PM, Vallabahajosula S, Goldsmith SJ, et al. In vitro characterization of radiolabeled monoclonal antibodies specific for the extracellular domain of prostate-specific membrane antigen. *Cancer Res.* 2000;60:5237–5243.
7. Bander NH, Nanus DM, Milowsky MI, Kostakoglu L, Vallabahajosula S, Goldsmith SJ. Targeted systemic therapy of prostate cancer with a monoclonal antibody to prostate-specific membrane antigen. *Semin Oncol.* 2003;30:667–676.
8. Hamilton A, King S, Liu H, Moy P, Bander N, Carr F. A novel humanized antibody against prostate specific membrane antigen (PSMA) for in vivo targeting and therapy [abstract]. *Proc Am Assoc Cancer Res.* 1998;39:440.
9. Smith-Jones PM, Vallabhajosula S, Navarro V, Bastidas D, Goldsmith SJ, Bander NH. Radiolabeled monoclonal antibodies specific to the extracellular domain of prostate-specific membrane antigen: preclinical studies in nude mice bearing LNCaP human prostate tumor. *J Nucl Med.* 2003;44:610–617.
10. Bander NH, Trabulsi EJ, Kostakoglu L, et al. Targeting metastatic prostate cancer with radiolabeled monoclonal antibody J591 to the extracellular domain of prostate specific membrane antigen. *J Urol.* 2003;170:1717–1721.
11. Liu H, Moy P, Kim S, et al. Monoclonal antibodies to the extracellular domain of prostate-specific membrane antigen also react with tumor vascular endothelium. *Cancer Res.* 1997;57:3629–3634.
12. Nanus DM, Milowsky MI, Kostakoglu L, et al. Clinical use of monoclonal antibody HuJ591 therapy: targeting prostate specific membrane antigen. *J Urol.* 2003;170(suppl):S84–S89.
13. Vallabhajosula S, Kuji I, Hamacher KA, et al. Pharmacokinetics and biodistribution of ^{111}In- and ^{177}Lu-labeled J591 antibody specific for prostate-specific membrane antigen: prediction of ^{90}Y-J591 radiation dosimetry based on ^{111}In or ^{177}Lu? *J Nucl Med.* 2005;46:634–641.
14. Bander NH, Milowsky MI, Nanus DM, Kostakoglu L, Vallabhajosula S, Goldsmith SJ. Phase I trial of ^{177}lutetium-labeled J591, a monoclonal antibody to prostate-specific membrane antigen, in patients with androgen-independent prostate cancer. *J Clin Oncol.* 2005;23:4591–4601.
15. Morris MJ, Divgi CR, Pandit-Taskar N, et al. Pilot trial of unlabeled and indium-111-labeled anti-prostate-specific membrane antigen antibody J591 for castrate metastatic prostate cancer. *Clin Cancer Res.* 2005;11:7454–7461.
16. Morris MJ, Pandit-Taskar N, Divgi CR, et al. Phase I evaluation of J591 as a vascular targeting agent in progressive solid tumors. *Clin Cancer Res.* 2007;13:2707–2713.
17. Barrett PH, Bell BM, Cobelli C, et al. SAAM II: simulation, analysis, and modeling software for tracer and pharmacokinetic studies. *Metabolism.* 1998;47: 484–492.
18. Stabin MG, Sparks RB, Crowe E. OLINDA/EXM: the second-generation personal computer software for internal dose assessment in nuclear medicine. *J Nucl Med.* 2005;46:1023–1027.
19. Sgouros G. Bone marrow dosimetry for radioimmunotherapy: theoretical considerations. *J Nucl Med.* 1993;34:689–694.
20. Bardiès M, Chatal JF. Absorbed doses for internal radiotherapy from 22 beta-emitting radionuclides: beta-dosimetry of small spheres. *Phys Med Biol.* 1994; 39:961–981.
21. Gonen M, Panageas KS, Larson SM. Statistical issues in analysis of diagnostic imaging experiments with multiple observations per patient. *Radiology.* 2001; 221:763–767.
22. O'Donoghue JA, Baidoo N, Deland D, Welt S, Divgi CR, Sgouros G. Hematologic toxicity in radioimmunotherapy: dose-response relationships for I-131 labeled antibody therapy. *Cancer Biother Radiopharm.* 2002;17:435–443.